CONFERENCE PRE-PRINT

PERFORMANCE EVALUATION OF TUNGSTEN FIBER-REINFORCED TUNGSTENCOMPOSITES DEVELOPED AT SWIP FOR APPLICATION IN NUCLEARFUSION REACTORS

Evaluation of Helium Retention Behavior in Tungsten Fiber-Reinforced Tungsten Plasma-Facing Materials

Zhao Tianyu^{1,2}, Wen Pan¹, Du Juan^{1,*}, Xu Shaoqiang¹, Li Jialin¹, Tang Jun²

- 1 Southwestern Institute of Physics, Chengdu 610000, China
- 2 Key Laboratory of Radiation Physics and Technology of Ministry of Education, Institute of Nuclear Science and Technology, Sichuan University, Chengdu 610064, China
- *corresponding author E-mail addresses: <u>dujuan@swip.ac.cn</u>

Abstract

When helium enters plasma-facing materials (PFMs), it undergoes a complex "self-trapping" phenomenon and mainly exists in the form of helium bubbles. The formation of helium bubbles exerts a significant impact on the microstructure and mechanical properties of PFMs, which is usually destructive. Therefore, in this study, leveraging the chemical inertness of helium ions, we introduced them into the interior of tungsten fiber-reinforced tungsten materials (W_f/W_m) via ion implantation technology, and investigated the distribution characteristics of helium bubbles in the materials. The results show that with the increase in helium ion implantation fluence, the size of helium bubbles W_f/W_m increases from 0.96 nm to 1.21 nm, and the number density doubles. At a helium ion implantation fluence of 2×10^{17} ions/cm², helium bubbles in ITER-grade tungsten are not only distributed closer to the surface but also form "nanocracks" inside the material, which are composed of dense helium bubbles. This phenomenon is expected to affect the "fuzz" structures on the material surface as well as void swelling. At this point, although helium causes less damage to the W_f/W_m samples than to the ITER-grade tungsten samples, the size and number density of helium bubbles in the W_f/W_m does not possess significant advantages in inhibiting the formation and growth of helium bubbles.

Key Words: Nuclear fusion, Tungsten fiber-reinforced tungsten, Plasma facing materials, Irradiation damage

1. INTRODUCTION

After deuterium and tritium plasmas undergo nuclear fusion reactions, the products include helium in addition to neutrons. Due to its extremely low solubility but high diffusion coefficient in tungsten, helium triggers a complex "self-trapping" phenomenon upon entering tungsten materials, and mainly exists in the form of helium bubbles ^[1]. The retention of these helium bubbles in the material, as well as their growth and movement with increasing irradiation fluence or changes in temperature—especially the helium fuzz phenomenon formed on the material surface after helium bubble rupture—exerts a significant and unique impact on the material's surface structure and properties ^[3-5].

In this paper, aiming at the tungsten fiber-reinforced tungsten material (W_f/W_m) developed in the early stage, we carried out helium ion implantation experiments, for the purpose of investigating the performance of W_f/W_m under He ion irradiation. With the aid of Transmission Electron Microscopy (TEM) tests, we conducted an indepth investigation into the distribution characteristics and retention behavior of helium in the material, providing important basic performance data support for the potential application of W_f/W_m .

2. EXPERIMENTAL MATERIALS AND METHODS

 W_{f}/W_{m} samples (see Reference 6 for specific fabrication methods) were cut into disks with a diameter of 12 mm and a thickness of 2 mm using a wire electrical discharge machine ^[6]. The disks were ground and polished, followed by vacuum annealing at 1000°C for 1 hour to eliminate residual stresses during machining process. ITER-grade rolled tungsten (supplied by ATTL Advanced Materials Co.,Ltd., China) underwent the same treatment and was used as the reference material for the experiment.

The helium ion irradiation experiments were conducted using an ion implanter at the Institute of Nuclear Science and Technology, Sichuan University. The implantation energy was 50 keV, and the total helium ion implantation fluences were 5×10^{16} ions/cm², 1×10^{17} ions/cm², and 2×10^{17} ions/cm², respectively.

To conduct an in-depth study on the characteristics of helium bubbles in the samples after helium implantation, we employed Focused Ion Beam (FIB) technology to perform precise cutting on the samples, starting from the helium-implanted surface. Subsequently, high-resolution imaging of the helium bubbles in the samples was carried out using the under-focus and over-focus modes of a Transmission Electron Microscope (TEM). Finally, with the aid of Nano Measure software, statistical analysis was performed on the sizes of the helium bubbles, and their volume density was calculated. This approach quantified the microstructural characteristics of helium, thereby facilitating comparisons of performance differences among various samples.

3. RESULTS AND DISCUSSION

In practical applications of PFMs, phenomena such as bubbles, fuzz, and pores can appear on their surfaces, which are the main forms of helium-induced damage in materials. Therefore, in this paper, we focus on using FIB technology to perform precise cutting of the ion-implanted regions. This method allows us to directly observe the characteristic changes of helium bubbles in the near-surface regions of materials under different implantation doses. Although this research scheme increases the experimental cost, it can provide us with more intuitive images, helping us to more clearly understand the helium retention characteristics in W_f/W_m PFMs. Consequently, it provides an important basis for optimizing material performance and extending their service life.

3.1. Helium ion implantation depth distribution and displacement Damage

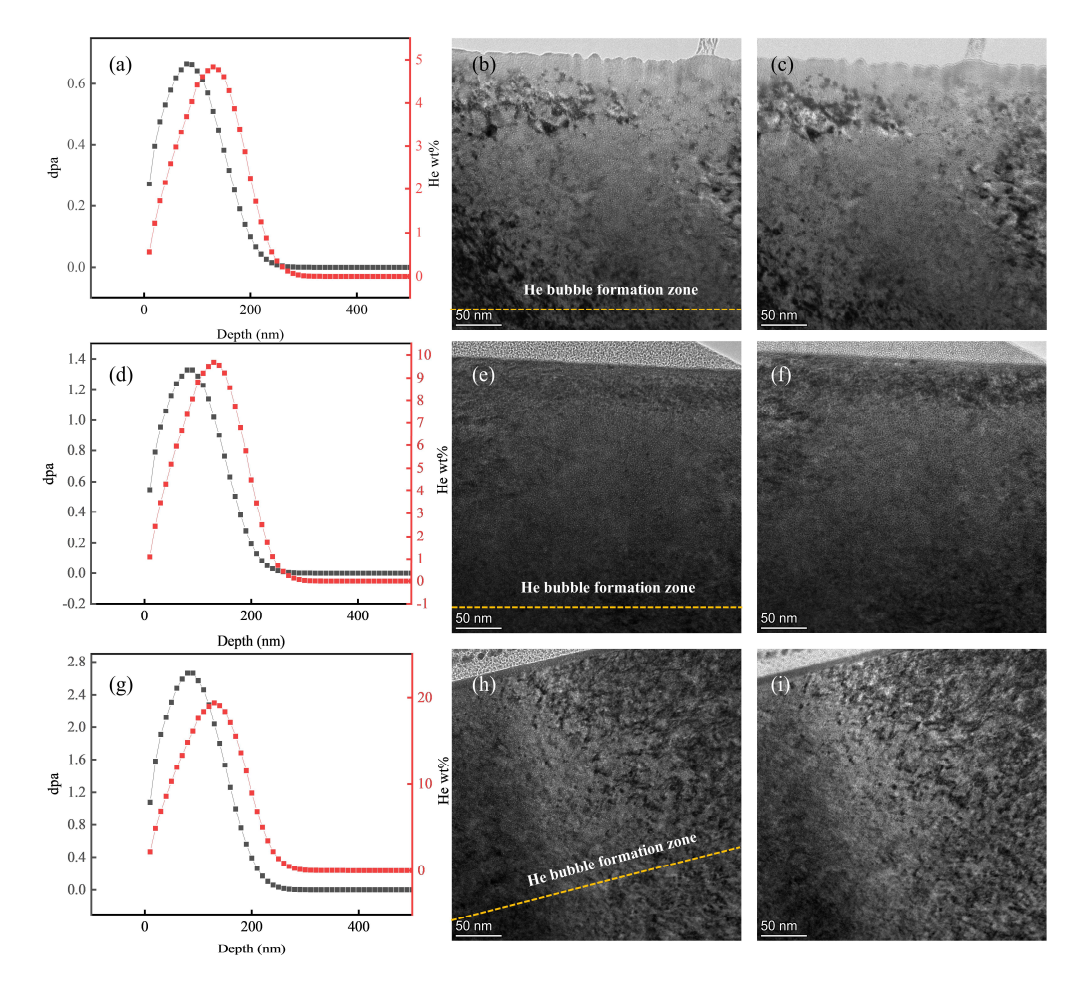


FIG. 1 Helium ion concentration distribution and displacement damage in W_f/W_m (a) SRIM simulation results; (b) TEM under-focused image; (c) TEM over-focused images; corresponding to an ion implantation dose of 5×10^{16} ions/cm². (d)-(e) correspond to the results when the ion implantation dose is increased to 1×10^{17} ions/cm². (g)-(i) correspond to the results when the ion implantation dose is increased to 2×10^{17} ions/cm².

Fig. 1 shows the distribution of helium ions in W_f/W_m under helium ion implantation fluences of 5×10^{16} ions/cm², 1×10^{17} ions/cm², and 2×10^{17} ions/cm². Among these, Figs. 1(a), (d), and (g) present the simulated distributions of displacement damage and helium concentration in the samples using SRIM software. The remaining figures display the distribution and characteristics of helium bubbles captured by TEM under the corresponding implantation fluences. Since helium bubbles in tungsten materials are extremely small (typically at the nanoscale), under-focus and over-focus TEM imaging techniques were employed to achieve more accurate localization and observation of the bubbles. For under-focus imaging, the focal point of the electron beam in the TEM is positioned in front of the sample. This results in more pronounced Fresnel Fringes at the edges of helium bubbles, enhancing the bubble boundary features and facilitating the observation of bubble distribution. In contrast, for over-focus imaging, the electron beam's focal point is located behind the sample, causing Fresnel Fringes to appear inside the helium bubbles. This reduces the contrast at the bubble edges, leading to a blurrier overall boundary definition compared to under-focus images. However, compared with under-focus images, over-focus images are more similar to in-focus images, making them more realistic and accurate for statistical analysis of helium bubble sizes.

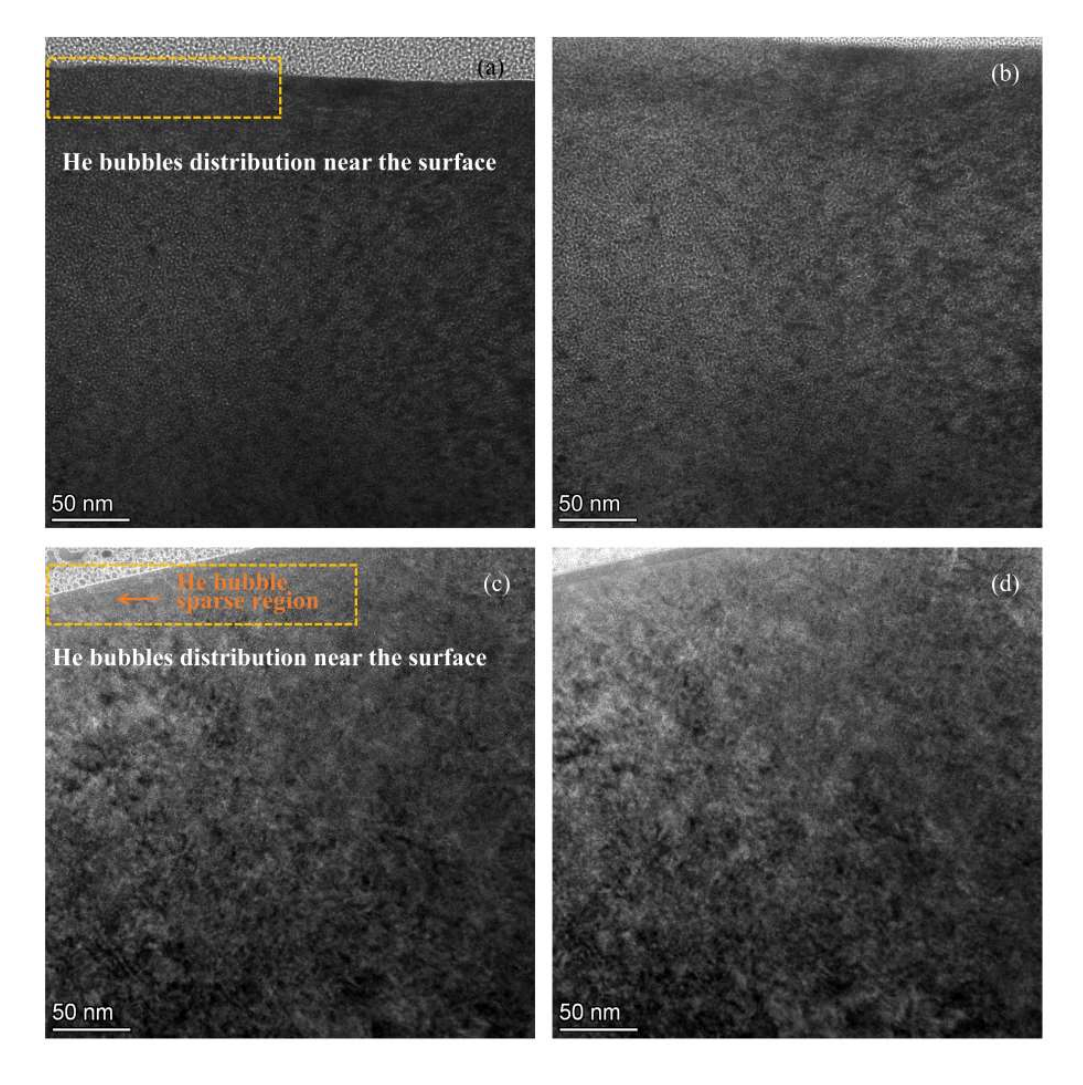


FIG. 2 Differences in the distribution of helium bubbles
(a) and (b) TEM under-focused image ITER-W; (c) and (d) TEM over-focused image Wf/Wm; with an ion fluence of 2*10¹⁷ ions/cm².

From the SRIM simulation results, it can be observed that the displacement damage to the material caused by ion implantation increases progressively, reaching a maximum of approximately 2.7 dpa (displacements per atom). The helium ions are distributed in a relatively shallow region: the peak of the helium ion count is around 170 nm deep, and the maximum implantation depth is only 350 nm. Corresponding helium bubble bands are also clearly visible in the TEM images; however, further magnification is required to accurately count the specific size and number density of the helium bubbles.

Meanwhile, characterization was also performed on ITER-W samples implanted with a helium fluence of 2×10^{17} ions/cm². Fig. 2 illustrates the differences in helium bubble distribution between these ITER-grade tungsten samples and the W_f/W_m samples. The results indicate that compared with W_f/W_m , the helium bubble bands in ITER-W are located significantly closer to the sample surface. In the W_f/W_m , although helium bubbles are present in the near-surface region, their density is lower, and there is a distinct with relatively sparse helium bubbles between the near-surface area and the main helium bubble band.

Helium bubbles closer to the surface are more prone to rupture because the material above them is thinner and has lower tensile strength, becoming sources of pores or fuzz defects. Simulation studies have shown that compared to deeper helium bubbles, helium bubbles located 1.5 nm below the titanium surface undergo morphological transformation and rupture rapidly after a period of relaxation. It is evident that under the same ion implantation fluence, excessive proximity of helium bubbles to the surface serves as a significant warning regarding changes in the surface radiation resistance of PFMs.

3.2. Size and number density of helium bubbles

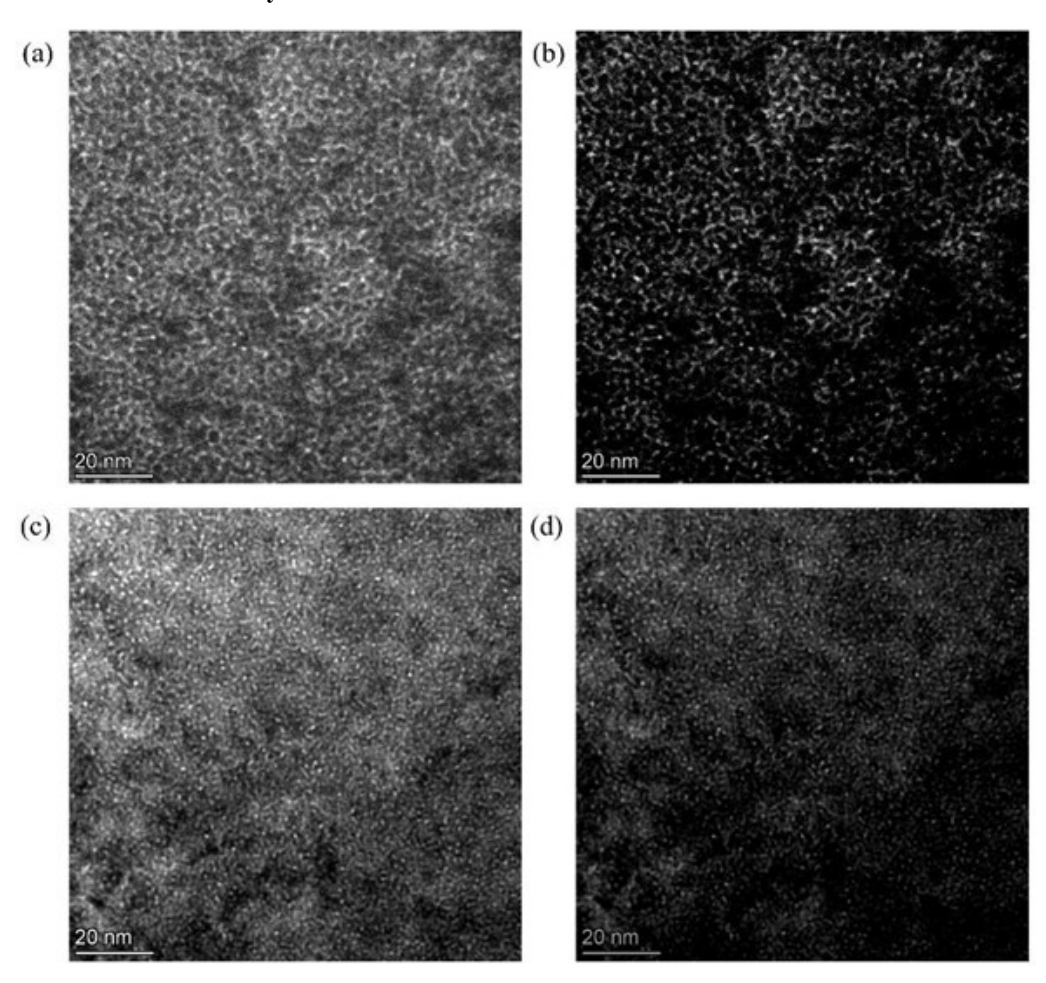


FIG. 3 Morphology and size of helium bubbles at a position 150 nm away from the sample surface (a) and (b) Under-focused photos of helium bubbles in ITER-W and the under-focused photos processed by the Image-Pro Plus software; (c) and (d) Under-focused photos of helium bubbles in W_f/W_m and the under-focused photos processed by the Image-Pro Plus software.

In order to compare the performance of W_f/W_m and ITER-W under helium implantation, we used a TEM to capture morphology images of helium bubbles at a uniform position 150 nm from the material surface. For samples with excessively thick TEM foils or high FIB-induced damage, we adjusted the contrast, brightness, and darkness using Image-Pro Plus software to improve image quality (see Fig. 3 for details).

The results show that helium bubbles in ITER-W have larger sizes and higher densities; most of the bubbles have coalesced, almost forming interconnected structures. Such interconnected structures have also been observed in

other research studies and termed "nanocracks". Since the spacing between helium bubbles in nanocracks is less than 2 nm, further growth in the size and quantity of helium bubbles will lead to the formation of void swelling. In contrast, under the same experimental conditions, helium bubbles in the W_f/W_m barely coalesced, demonstrating superior performance advantages.

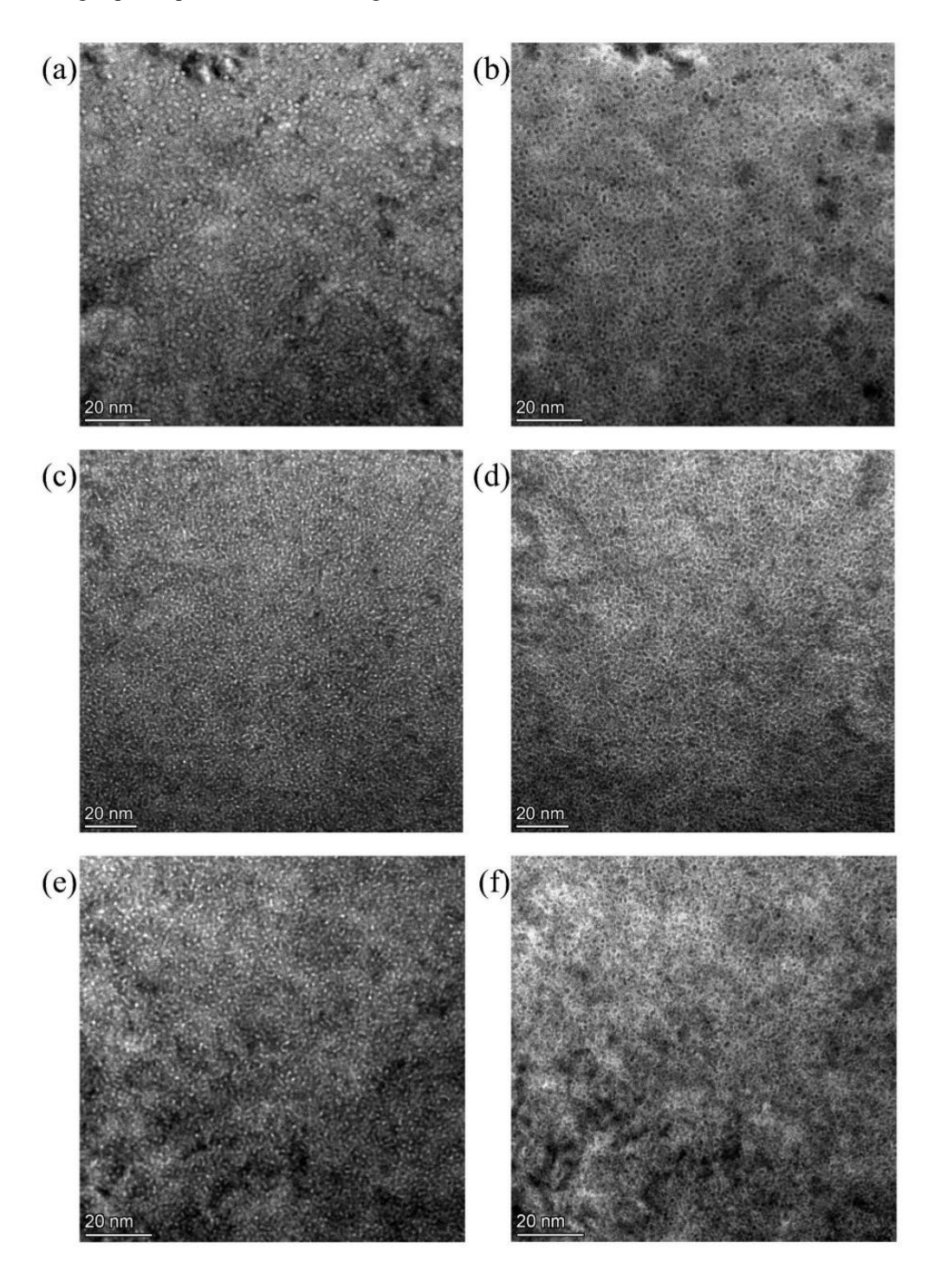


FIG. 4 Size and distribution of helium bubbles at a position 150 nm away from the sample surface of W_f/W_m (a) and (b) correspond to an ion implantation dose of $5*10^{16}$ ions/cm²; (c)-(d) correspond to an ion implantation dose of $1*10^{17}$ ions/cm²; (e)-(f) correspond to an ion implantation dose of $2*10^{17}$ ions/cm².

Fig. 4 shows the microtopography of W_f/W_m under different helium ion implantation fluences. With the aid of Nano Measure software, we were able to more accurately count and analyze the variations in the morphology and

IAEA-CN-336/INDICO ID 3364

quantity of helium bubbles as the implantation fluence increased, and summarize the corresponding laws based on this.

The statistical results of helium bubble size and number density are presented in Table 1. As the helium ion implantation fluence increased, the helium concentration in the samples continuously rose. At the maximum fluence, the central concentration of the helium bubble band reached 20%. Correspondingly, the helium bubble size increased from 0.96 nm at the low fluence to 1.17 nm at the medium fluence, and the tendency of size growth levelled off when the implantation fluence was further increased. Meanwhile, the number density of helium bubbles in the samples increased rapidly without showing a tendency to level off. However, compared with the reference material (ITER-W), the $W_{\rm f}/W_{\rm m}$ exhibited certain advantages in terms of helium bubble size and number density.

Table 1 Statistics of the Size and Number Density of Helium Bubbles

Sample Number	Implantation Fluence	Bubble Size	Bubble Number Density
	(cm ⁻²)	(nm)	(cm^3)
W_f/W_m -1	5×10 ¹⁶	0.96	7.5×10 ¹²
W_f/W_m -2	1×10^{17}	1.17	1.09×10^{13}
W_f/W_m -3	2×10 ¹⁷	1.21	1.45×10^{13}
ITER-W	2×10^{17}	1.45	1.72×10^{13}

4. CONCLUSION

With the increase in helium ion implantation fluence, the size of helium bubbles in W_f/W_m materials increases from 0.96 nm to 1.21 nm, and the number density doubles. At a helium ion implantation fluence of 2×10^{17} ions/cm², helium bubbles in ITER-W are not only distributed closer to the surface but also form "nanocracks" inside the material, which are composed of dense helium bubbles. This phenomenon is expected to affect the "fuzz" structures on the material surface as well as void swelling. At this point, although helium causes less damage to the W_f/W_m samples than to the ITER-W samples, the size and number density of helium bubbles in the W_f/W_m samples have reached approximately 85% of those in the ITER-W samples. This indicates that the W_f/W_m material does not possess significant advantages in inhibiting the formation and growth of helium bubbles.

ACKNOWLEDGEMENT

This study received fundings from the National Natural Science Foundation of China (NO.12375204) and TianFuEMei Innovation and Entrepreneurship Team Foundation (2023TFEMCXTD).

REFERENCES

- [1] Huang J, Li Y, Yuan G, et al. Corrosion and microstructure evolution of He+ plasma irradiated tungsten PFMs [J]. Fusion Engineering and Design, 2022, 184: 113279.
- [2] Juslin N, Wirth B D. Interatomic potentials for simulation of He bubble formation in W [J]. Journal of Nuclear Materials, 2013, 432(1-3): 61-6.
- [3] Woller K B, Whyte D G, Wright G M. Isolated nano-tendril bundles on tungsten surfaces exposed to radiofrequency helium plasma [J]. Nuclear Materials and Energy, 2017, 12: 1282-7.
- [4] Wang Q, Wang L, Wu C, et al. First-principles study on mechanical properties and retention behaviors of hydrogen in W by additions of Re and Mo [J]. International Journal of Hydrogen Energy, 2024, 49: 1506-13.
- [5] Xu S, Fan X, Gu C, et al. Molecular dynamics simulation of bubble growth under surface of tungsten under helium irradiation [J]. Journal of Nuclear Materials, 2023, 573: 154154.
- [6] Zhao T, Li J, Tang J,et al. Mechanical properties of a novel tungsten fiber-reinforced tungsten composite prepared through powder extrusion printing and high-pressure high-temperature sintering [J]. Nuclear Materials and Energy, 2023, 37: 101553.